Hindawi
International Journal of Photoenergy
Volume 2017, Article ID 8983717, 8 pages
https://doi.org/10.1155/2017/8983717

Research Article

One-Pot Solid-State Reaction Approach to Synthesize Ag-Cu_2O/GO Ternary Nanocomposites with Enhanced Visible-Light-Responsive Photocatalytic Activity

Longfeng Li,[1,2] Jing Zhang,[1] Xianliang Fu,[1] Peipei Xiao,[1] Maolin Zhang,[1,2] and Mingzhu Liu[1,2]

[1]*School of Chemistry and Materials Science, Huaibei Normal University, Huaibei 235000, China*
[2]*Information College, Huaibei Normal University, Huaibei 235000, China*

Correspondence should be addressed to Maolin Zhang; zhangml@chnu.edu.cn and Mingzhu Liu; once1970@sina.com

Received 7 December 2016; Accepted 29 January 2017; Published 28 March 2017

Academic Editor: Laécio S. Cavalcante

A facile ball milling-assisted solid-state reaction method was developed to synthesize Ag-Cu_2O/graphene oxide (GO) nanocomposites. In the resultant complex heterostructures, Ag nanocrystals were mainly deposited on the surface of Cu_2O, while Ag-Cu_2O composites were anchored onto GO sheets. The resultant Ag-Cu_2O/GO nanocomposites exhibited excellent photocatalytic activity with 90% of methyl orange (MO) dye degradation efficiency after 60 min of visible-light irradiation, which was much higher than that of either Cu_2O or Ag-Cu_2O. This study opens a new avenue to fabricate visible-light-responsive photocatalyst with high performance for environmental pollution purification.

1. Introduction

Developing visible-light-responsive photocatalysts for the extensive application in environmental pollution purification has attracted considerable concerns in recent years. Of the concerned photocatalysts, cuprous oxide (Cu_2O), a p-type semiconductor with a small direct band gap (1.9–2.2 eV), has been proved to be the most promising candidate for visible-light-driven photocatalytic decontamination [1–4]. Unfortunately, the rapid recombination of photogenerated electron-hole pairs greatly decreases its quantum efficiency and limits its promising applications in photocatalysis [5]. To prevent the recombination of photogenerated electron-hole pairs, several strategies such as doping with elements [6, 7] and coupling with other semiconductors [8, 9] have been developed to design and synthesize the desired Cu_2O-based composite materials, since it has been demonstrated that semiconductor-based composite/hybrid materials can display new synergistic properties arising from the interaction between the different components to improve the performances of the original semiconductors [10].

Among various strategies, constructing noble metal-semiconductor binary nanohybrids is an effective method for improving the photocatalytic activity. It is believed that the Schottky barrier created between metal and semiconductor can effectively prevent the recombination of photogenerated charge carriers during the photocatalytic process, resulting in an enhanced photocatalytic activity [11, 12]. To date, several binary metal/Cu_2O heterogeneous nanostructures such as Cu/Cu_2O [13], Au/Cu_2O [14, 15], and Ag/Cu_2O [16, 17] have been successfully prepared and have shown expected enhanced photocatalytic activities in degradation of organic dyes like MO [13, 16, 17], methylene blue (MB) [14], and pyronine B [15] compared to pure Cu_2O.

Although dual-ingredient metal/Cu_2O composites display an enhanced photocatalytic performance for photocatalytic degradation of organic pollutants compared to pure Cu_2O, multicomponent nanomaterials are expected to provide much higher photoactivity and to promote the development of novel nanoarchitectures with extraordinary properties [18]. Recent studies [19–21] have evidenced that the combined effect of graphene and plasmonic metals on the semiconductor

photocatalyst can effectively improve the photocatalytic activity via suppressing photogenerated electron-hole recombination and/or increasing the photoabsorption ability. For instance, Ahmad et al. [19] have introduced graphene to Mn-doped ZnO forming Mn-doped ZnO/graphene ternary nanocomposite photocatalysts using solvothermal method for photocatalytic degradation of MB under visible-light irradiation. They find that the as-synthesized Mn-doped ZnO/graphene ternary nanocomposite shows an impressive photocatalytic enhancement over Mn-doped ZnO or pure ZnO samples, which can be attributed to enhanced visible-light absorption, efficient charge separation, and fast transfer processes. Jin et al. [20] have fabricated Cu-P25-graphene ternary composite through hydrothermal method for photocatalytic degradation of MB. Compared to the pure P25 and the P25-graphene binary composite, the as-fabricated Cu-P25-graphene ternary composite exhibits extended visible-light absorption, good charge separation capability, and high degradation rate of MB under visible-light irradiation. Hsieh et al. [21] have constructed ternary Pt-TiO_2/graphene hybrids with higher visible-light-driven photocatalytic activities in degrading AO7 than TiO_2/graphene. To sum up, it will be beneficial to use the synergetic effect among graphene, metal, and semiconductor photocatalysts for improving visible-light absorption and photocatalytic activity.

Considering the advantages of the aforementioned types of photocatalysts, fabricating Ag-Cu_2O/graphene ternary composite may reveal some desirable properties for photocatalytic applications. However, at present, only one research [5] focuses on this kind of nanocomposite. And much work should be done to prepare Ag-Cu_2O/graphene ternary nanocomposites instead of binary nanomaterials for improving photocatalytic performance. On the other hand, a variety of methods such as solvothermal [19] and hydrothermal [20, 21] has been established to prepare metal-semiconductor/graphene ternary composites. These methods generally involve a multiple-step synthesis procedure, which is complicated and not suitable for mass production. Thus, a simple, high-yielding, and environmentally friendly method is highly desirable for the bulk production of this kind of ternary composites with high photocatalytic performance.

Compared to other methods for the preparation of nanomaterials, the ball milling-assisted solid-state reaction method has a simpler process, higher yield, and lower environmental impact, which has been reported in our previous work [4, 22]. Up to now, this method has not been used for the synthesis of Ag-Cu_2O/GO ternary nanocomposites. In this work, we first successfully synthesize Ag-Cu_2O/GO ternary nanocomposites via a facile ball milling-assisted solid-state reaction route. The photocatalytic performances of the as-synthesized Ag-Cu_2O/GO with various Ag loading amounts are investigated. The results indicate that all the ternary nanocomposites display much higher photocatalytic activity for the degradation of MO under visible-light irradiation than pure Cu_2O or Ag-Cu_2O binary composite. Our work may provide an alternative to synthesize visible-light-responsive ternary nanocomposites with high photocatalytic performance.

2. Experimental

2.1. Materials and Apparatus. $Cu_2(OH)_2CO_3$, $AgNO_3$, and $H_2C_2O_4{\cdot}2H_2O$ used in the study were of analytical grade quality, and graphene oxide nanoplatelets (thickness: 0.55–1.2 nm) were purchased from Beijing DK nano technology Co. LTD and used as received. An X-ray powder diffractometer (XRD; Bruker D8 Advance, Germany) with Cu Kα radiation ($\lambda = 0.15418$ nm), an accelerating voltage of 40 kV, and an emission current of 40 mA was used to determine the crystal phase composition and the crystallite size of the synthesized samples. A field-emission scanning electron microscope (FE-SEM; Hitachi S-4800, Japan), a high-resolution transmission electron microscope (HRTEM; JEOL JEM-2100, Japan), and a transmission electron microscope (TEM; HT7700, Japan) with an energy-dispersive X-ray spectroscopy system (EDS; Oxford Instruments, UK) were employed to observe the microstructures, morphology, and elemental composition of the as-synthesized samples.

2.2. Synthesis Procedure. In a typical synthesis process, $Cu_2(OH)_2CO_3$, $AgNO_3$, $H_2C_2O_4{\cdot}2H_2O$, and GO were firstly mixed together in a certain molar ratio. Then, the resultant mixtures were allowed to have a ball milling reaction for 1 h using the planetary ball mill (QM-3SP04, China) with zirconium oxide tanks at a rotation speed of 480 rpm at room temperature. Finally, the as-obtained intermediate product was calcined at 350°C for 1 h under the protection of nitrogen to get the Ag-Cu_2O/GO ternary nanocomposite. Following the same procedure, various Ag-Cu_2O/GO nanocomposites were synthesized at an $AgNO_3/Cu_2(OH)_2CO_3/H_2C_2O_4{\cdot}2H_2O$ molar ratio of $m : 1 : (1 + m)$ and a $Cu_2(OH)_2CO_3$/GO mass ratio of 50 : 1 and were termed as mAg-Cu_2O/GO (m was in the range of 0.02~0.2). Also, 0.1Ag-Cu_2O was prepared by removing GO from the starting materials, and pure Cu_2O was obtained by removing $AgNO_3$ and GO.

2.3. Photocatalytic Activity Measurement. The photocatalytic degradation experiments were carried out in a photochemical reactor using a 300 W Xe lamp with a 420 nm UV cutoff filter, and the photocatalytic performances of the as-synthesized mAg-Cu_2O/GO nanocomposites with m values of 0.04, 0.06, 0.1, and 0.2 were evaluated by the photocatalytic degradation of the MO solution. The reaction temperature was kept at room temperature by cooling water to prevent any thermal catalytic effect. In a typical photocatalytic experiment, 0.25 g of the mAg-Cu_2O/GO powder was first added into 100 ml of the MO solution (20 mg l^{-1}). Then, prior to light irradiation, the resultant solution was magnetically stirred in the dark for approximately 30 min to ensure the adsorption-desorption equilibrium between the catalyst and the MO molecules. Next, the resultant solution was exposed to Xe lamp irradiation. Finally, a 5.0 ml reaction suspension including the photocatalyst and MO was withdrawn and centrifuged to separate the photocatalyst at 15 min intervals. The degradation rate of MO was evaluated by recording the intensity of absorption peak of MO (464 nm) relative to its initial intensity (c/c_0) using a spectrophotometer. The details were referred to our recent work [22]. Following the same

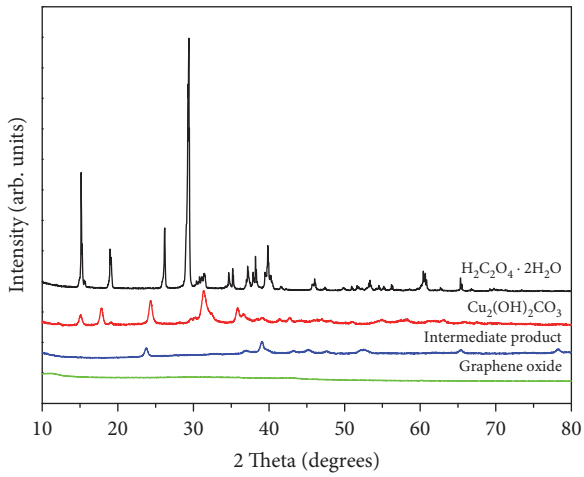

Figure 1: XRD patterns of the reactants and intermediate product.

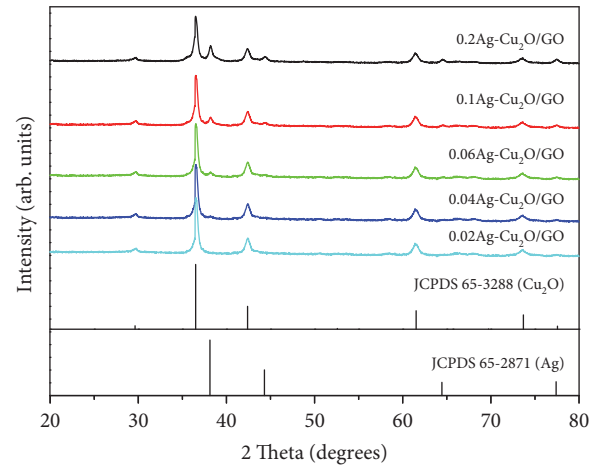

Figure 2: XRD patterns of mAg-Cu_2O/GO nanocomposites synthesized with different m values.

procedures, photocatalytic activities of pure Cu_2O, GO, and 0.1Ag-Cu_2O powders were also investigated for comparison with those of the mAg-Cu_2O/GO nanocomposites.

3. Results and Discussion

3.1. Principle of Synthesis Route. The synthesis of mAg-Cu_2O/GO nanocomposites is a two-stage process. At the first stage, the mixed reactants are ball milled for 1 h, which allows the solid-state reaction among $H_2C_2O_4{\cdot}2H_2O$, $Cu_2(OH)_2CO_3$, and $AgNO_3$, forming the intermediate product of $1/2\ m{Ag_2C_2\ \ O_4} - Cu_2(OH)_{2n}(NO_3)_m(CO_3)_{1-n-m}(C_2O_4)_{1+1/2m}$ ($n = 0{\sim}1$) deposited on the surface of GO. At the second stage, the resultant intermediate product undergoes thermal decomposition reaction under the protection of nitrogen atmosphere at 350°C, which is an intramolecular redox reaction because of the reducibility of $C_2O_4^{2-}$ and the oxidizability of Cu^{2+}, to obtain Ag-Cu_2O/GO sample. The formation of Ag-Cu_2O/GO is represented by the following chemical equations:

$$\begin{aligned} &m\mathrm{AgNO_3}(s) + \mathrm{Cu_2(OH)_2CO_3}(s) + (1+m)\mathrm{H_2C_2O_4} \\ &\quad \cdot 2\mathrm{H_2O}(s) + \text{graphene oxide} \xrightarrow{\text{Ball milling}} \\ &\quad \frac{1}{2}m\mathrm{Ag_2C_2O_4} - \mathrm{Cu_2(OH)_{2n}(NO_3)_m} \\ &\quad (\mathrm{CO_3})_{1-n-m}(\mathrm{C_2O_4})_{1+1/2m}/\mathrm{GO} + (4+2m-2n) \\ &\quad \mathrm{H_2O}(l) + (n+m)\mathrm{CO_2}(g) \end{aligned} \tag{1}$$

$$\begin{aligned} &\frac{1}{2}m\mathrm{Ag_2C_2O_4} - \mathrm{Cu_2(OH)_{2n}(NO_3)_m(CO_3)_{1-n-m}(C_2O_4)_{1+1/2m}} \\ &\quad /\mathrm{GO} \xrightarrow{\text{Calcination } (350^\circ\mathrm{C},\ \mathrm{N_2})} m\mathrm{Ag} - \mathrm{Cu_2O/GO} \\ &\quad + n\mathrm{H_2O}(g) + (3+m-n)\mathrm{CO_2}(g) + m\mathrm{NO_2}(g) \end{aligned} \tag{2}$$

The XRD patterns of the initial reactants and the intermediate product, which is obtained in the molar ratio of 0.1 : 1 : 1.1 of $AgNO_3$, $Cu_2(OH)_2CO_3$, and $H_2C_2O_4{\cdot}2H_2O$ after 1 h of ball milling, are presented in Figure 1. It can be seen that the diffraction peaks of the initial reactants completely disappear in the intermediate product, and those of the new phases appear, indicating that the solid-state reaction of $H_2C_2O_4{\cdot}2H_2O$, $Cu_2(OH)_2CO_3$, and $AgNO_3$ is completed after 1 h of ball milling.

3.2. Phase Structures of mAg-Cu_2O/GO. Figure 2 shows the X-ray diffraction patterns of mAg-Cu_2O/GO nanocomposites synthesized with different molar ratios of $AgNO_3$ to $Cu_2(OH)_2CO_3$. It is found that the diffraction peaks of all the products match well with those of cubic Cu_2O (JCPDS 65-3288), and the characteristic diffraction peaks of Ag (JCPDS 65-2871) also appear in 0.06Ag-Cu_2O/GO, 0.1Ag-Cu_2O/GO, and 0.2Ag-Cu_2O/GO products, whose diffraction peak intensity gradually increases with an increase in the amount of $AgNO_3$. Besides, no signals of impurities are observed in all the products. Based on Scherrer's equation, the mean crystallite sizes of Cu_2O in mAg-Cu_2O/GO composites are calculated and are about 48, 44, 40, 36, and 31 nm corresponding to the m values of 0.02, 0.04, 0.06, 0.1, and 0.2, respectively, while those of Ag are about 5, 7, and 10 nm corresponding to the m values of 0.06, 0.1, and 0.2, respectively. The results indicate that, with the increase in the amount of $AgNO_3$, the crystallite sizes of Cu_2O in the composites gradually decrease, while those of Ag gradually increase.

3.3. Morphology and Microstructure. The morphology and microstructure of the 0.1Ag-Cu_2O/GO nanocomposite are examined by SEM and TEM as illustrated in Figure 3. It can be seen that spherical-like or nearly cubic-like Ag-Cu_2O particles with little aggregation are attached to the GO sheet, and most of the small Ag nanoparticles are directly deposited on the surface of Cu_2O particles with a size range of 45–70 nm (Figures 3(a) and 3(b)). The microstructure of 0.1Ag-Cu_2O/GO nanocomposite is further investigated by HRTEM. As shown in the HRTEM image (Figure 3(c)), Ag-Cu_2O interfaces are clearly observed and the observed interplanar spacings of 0.25 and 0.24 nm will correspond to

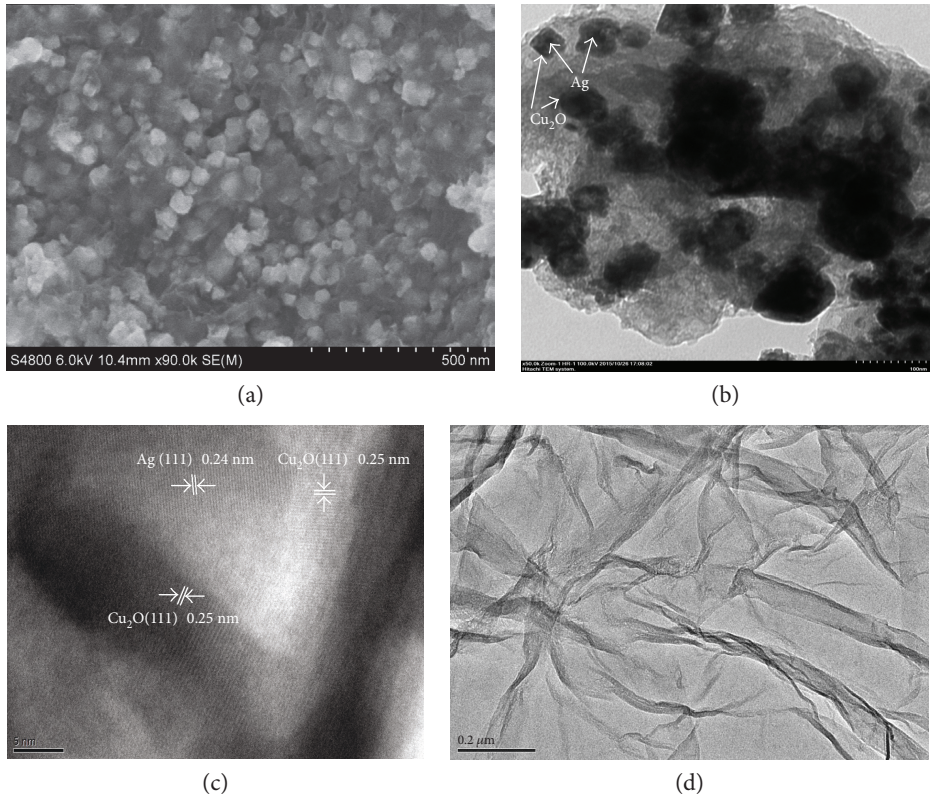

Figure 3: SEM (a), TEM (b), and HRTEM (c) images of 0.1Ag-Cu_2O/GO and TEM (d) image of GO.

the (111) lattice planes of Cu_2O and Ag, respectively, confirming that Ag nanocrystals are successfully anchored on the surfaces of Cu_2O.

To further observe the composition and the distribution of various elements, the EDS analyses of 0.1Ag-Cu_2O/GO are also performed. EDS analyses in the scanning transmission electron microscopy (STEM) mode have shown the presence of Ag, Cu, O, and C elements in the Ag-Cu_2O/GO composites, as shown in Figure 4. The EDS spectrum in Figure 4(a2) indicates that the marked area in Figure 4(a1) contains 57.7 wt% C, 11.9 wt% O, 27.9 wt% Cu, and 2.5 wt% Ag. That is, the atomic ratio of Cu to Ag is about 18.94 : 1, which is in agreement with the theoretical value of 20 : 1 in 0.1Ag-Cu_2O/GO. In contrast, another selected area for EDS analysis is located at the Ag deposition region on an individual Ag-Cu_2O nanoparticle (Figure 4(b1)) and the EDS spectrum indicates that the selected area contains 20 wt% C, 3.9 wt% O, 30.8 wt% Cu, and 45.3 wt% Ag (Figure 4(b2)). Through data calculation conversion, the atomic ratio of Cu to Ag is about 1.15 : 1 in the selected area in Figure 4(b1). It is seen that, compared with that in Figure 4(a1), the selected area in Figure 4(b1) is rich of Ag, which provides further evidence that the small Ag nanocrystalline is directly deposited on the surface of Cu_2O nanoparticles. In order to analyze the distribution of each element in the sample, EDS image scanning is performed on the framed area in Figure 4(c1) and the elemental maps of Cu, O, C, and Ag are shown in Figures 4(c2), 4(c3), 4(c4), and 4(c5), respectively. As can be seen, C element signals cover the entire selected area (Figure 4(c4)), suggesting that they are mainly from the GO. The distribution of Cu, O, and Ag elements, in particular, that of Cu and Ag elements, basically corresponds to the STEM image of 0.1Ag-Cu_2O, suggesting that they are mainly from the 0.1Ag-Cu_2O. Therefore, combining the results of XRD, SEM, TEM, and EDS, it can be concluded that the ternary Ag-Cu_2O/GO nanocomposites have been successfully synthesized.

3.4. Photocatalytic Activities and Mechanism. The photocatalytic activities of *m*Ag-Cu_2O/GO with different Ag loading amounts ($m = 0.04$, 0.06, 0.1, and 0.2) are evaluated in terms of the degradation rate of MO in aqueous solution under visible-light irradiation, and experimental results are shown in Figure 5. For comparison, the test results of pure Cu_2O, GO, and 0.1Ag-Cu_2O are also displayed in Figure 5. Obviously, the photolysis of MO is negligible in the absence of the photocatalyst and pure GO exhibits 9.7% photocatalytic degradation efficiency for MO after 60 min of visible-light irradiation, suggesting its low photocatalytic activity. Besides, the photocatalytic degradation efficiency of pure Cu_2O is up to 64%, while 0.1Ag-Cu_2O is up to 78%. Acting as electron sinks, Ag nanoparticles deposited on Cu_2O can reduce the recombination of the photoinduced carriers, resulting in better photocatalytic activity of 0.1Ag-Cu_2O than pure Cu_2O. It is worth mentioning that all the Ag-Cu_2O/GO ternary nanocomposites exhibit excellent photocatalytic activities, which are much higher than those of either pure Cu_2O or Ag-Cu_2O binary composites. Moreover, the photocatalytic activities of the *m*Ag-Cu_2O/GO increase slightly with increasing Ag loading amounts from 0.04

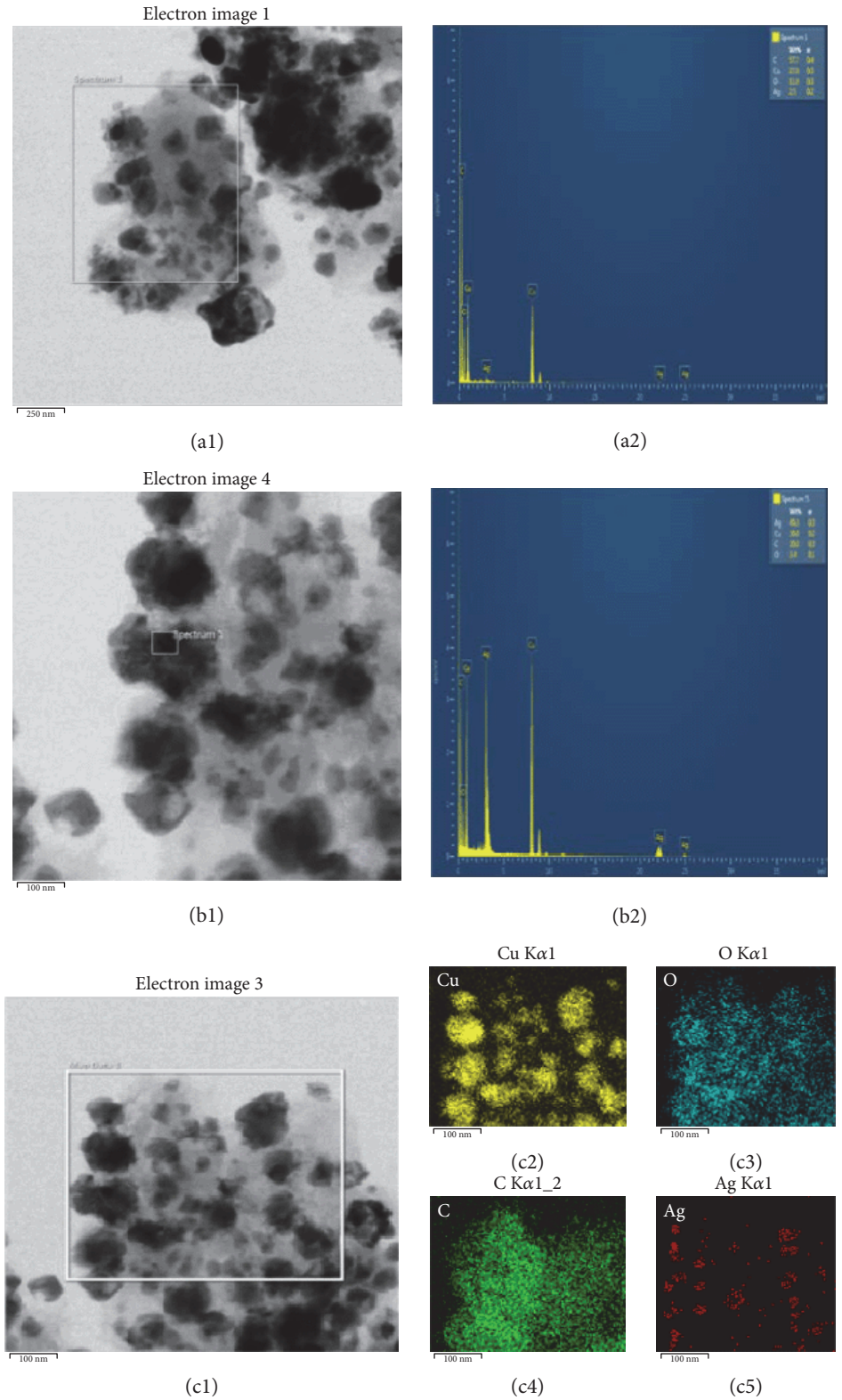

FIGURE 4: EDS analyses of 0.1Ag-Cu_2O/GO. STEM images (a1), (b1), and (c1), EDS spectra (a2) and (b2), and elemental maps (c2), (c3), (c4), and (c5).

to 0.1 of m values and the degradation percentage of MO follows the order of 0.1Ag-Cu_2O/GO (90%) > 0.06Ag-Cu_2O/GO (85%) > 0.04Ag-Cu_2O/GO (83%) after 60 min of visible-light irradiation. Interestingly, after the Ag loading amount reaches 0.2 of m value, the photocatalytic activity of 0.2Ag-Cu_2O/GO decreases slightly. Therefore,

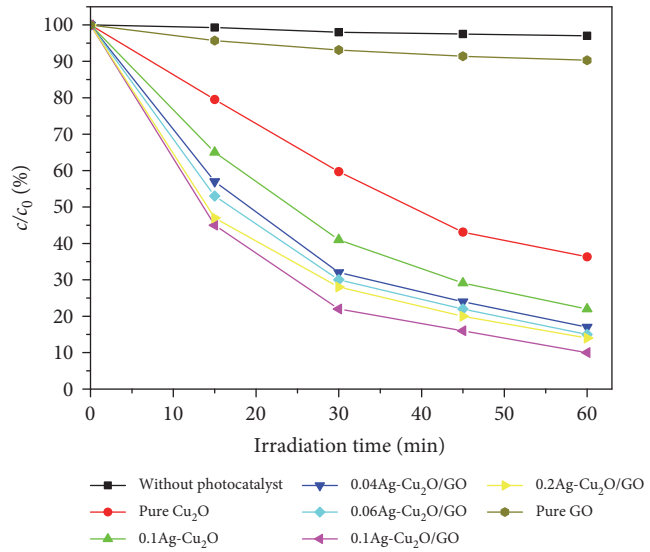

Figure 5: Photocatalytic degradation of MO under visible-light irradiation with different photocatalysts.

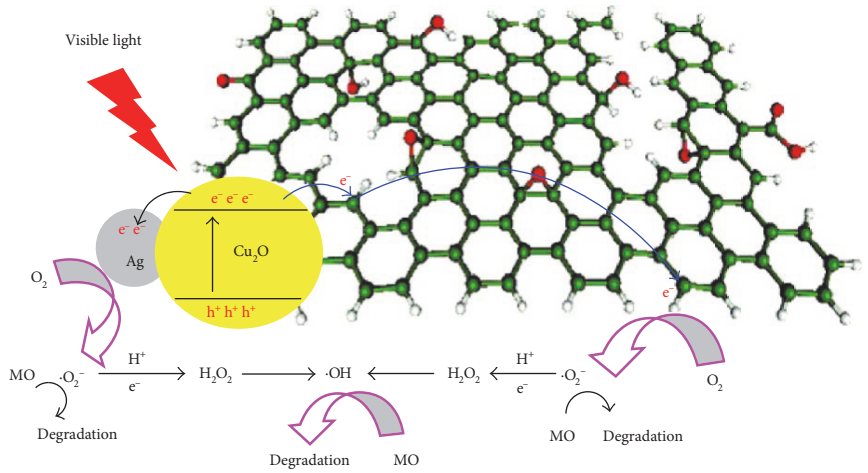

Figure 6: Schematic illustration of the charge transfer in Ag-Cu_2O/GO composite.

0.1 of m value is the optimal loading content of Ag and the higher content of Ag could be detrimental to the photocatalytic efficiency. It is due to its high content that Ag may serve as a new recombination center between photogenerated electrons and holes, thus reducing the photocatalytic activity of the photocatalyst [23]. In addition, the stability and reusability of 0.1Ag-Cu_2O/GO are evaluated over its multiple cycles for the photocatalytic degradation of MO. Stability tests are performed by repeating the reaction five times with the cycle length of 60 min using the recovered photocatalyst, and the degradation percentage of MO is about 89% at the end of the fifth cycle, which reveals that there is a negligible decrease in photocatalytic activity up to five cycles. So, 0.1Ag-Cu_2O/GO ternary nanocomposite prepared in the present work is a highly stable and reusable photocatalyst.

As expected, all the Ag-Cu_2O/GO nanocomposites show higher photocatalytic activities in the degradation of MO compared to the pure Cu_2O or the Ag-Cu_2O binary composite. It generally can be ascribed to a positive synergetic effect between various components. First of all, GO plays important roles in improving the visible-light-driven photocatalytic performance, which are described as follows: (1) the strong adsorption of GO to MO molecules resulting from the special π-conjugation and larger surface area of GO results in a high concentration of MO on the surface or in the vicinity of Ag-Cu_2O deposited on GO and thus increases the reaction rate. (2) GO with good electrical conductivity can act as an electron sink due to its higher work function than 4.42 eV of grapheme, and the existence of π-bands in GO facilitates charge transfer along the π-system [24], which accelerates electron transfer from Cu_2O to GO and further transfer to electronic receivers, leading to an improvement in the separation efficiency of the photoinduced carriers. Thereby, the higher photocatalytic performance of Ag-Cu_2O/GO ternary composites can be achieved. Apart from GO, Ag nanoparticles are also

responsible for the higher photocatalytic performance of Ag-Cu_2O/GO ternary composites because they can also act as electron sinks to prevent the recombination of the photogenerated electrons and holes. And synergetic effects among different components for the superior photocatalytic activity of Ag-Cu_2O/GO ternary nanocomposites are illustrated in Figure 6. The valence band (VB) and the conduction band (CB) of Cu_2O with a band gap of about 1.94 eV in the composite are estimated to be about 0.5 eV and −1.44 eV versus normal hydrogen electrode (NHE) (pH = 0), respectively [25]. When Ag-Cu_2O/GO is under visible-light irradiation, the photoinduced electrons (e^-) will transfer from CB of Cu_2O to GO or Ag deposited on Cu_2O and then GO with superior conductivity will transfer these electrons along the π-system to the liquid/GO interface, while Ag nanoparticles with photoexcited plasmonic metallic nanostructure can extend the lifetime of electrons that arrived on its surface, which are crucial for the electron-dominated reduction reaction. At the liquid/GO interface or on the surface of Ag nanoparticles, the dissolved oxygen (O_2) in water acting as the electron scavenger can be reduced by trapping electrons to superoxide radical anions (O_2^-) and is further converted into hydrogen peroxide (H_2O_2) and hydroxyl radical (·OH). Then, hydroxyl radicals and superoxide radical anions acting as very powerful oxidants will oxidize MO molecules into small molecules such as CO_2 and H_2O. Therefore, combining photocatalytically active Cu_2O with GO acting as the electron sink and the adsorbent, as well as Ag nanoparticles acting as electron traps, can contribute to an effective photocatalytic degradation of MO under visible-light irradiation.

4. Conclusions

In this study, various Ag-Cu_2O/GO ternary nanocomposites as novel visible-light-responsive photocatalysts have been synthesized via a simple ball milling-assisted solid-state reaction route for the first time. Compared to the pure Cu_2O and the Ag-Cu_2O binary nanocomposite, the as-synthesized Ag-Cu_2O/GO ternary nanocomposites show superior visible-light-driven photocatalytic activity for MO degradation. The excellent photocatalytic activity of Ag-Cu_2O/GO can be attributed to the following facts: (1) the strong adsorption of GO to MO molecules results in increasing reaction rate of photocatalytic degradation; (2) good electrical conductivity and π-bands of GO are in favor of charge transfer, reducing the recombination of the photogenerated charge carriers; (3) Ag nanoparticles serve as electron sinks, accelerating the photoinduced charge carrier separation. The excellent performance of the Ag-Cu_2O/GO photocatalyst enables it to be used as a promising candidate in the field of environmental pollution purification. Also, this study provides a facile synthetic route for the synthesis of visible-light-responsive ternary nanocomposites with high photocatalytic performance.

Conflicts of Interest

The authors declare that they have no competing interest.

Acknowledgments

This work is financially supported by the Natural Science Foundation of Anhui Provincial Education Department (KJ2016A640, KJ2017A841, and KJ2013B249).

References

[1] X. Q. Liu, Z. Li, W. Zhao, C. X. Zhao, Y. Wang, and Z. Q. Lin, "A facile route to the synthesis of reduced graphene oxide-wrapped octahedral Cu_2O with enhanced photocatalytic and photovoltaic performance," *Journal of Materials Chemistry A*, vol. 3, no. 37, pp. 19148–19154, 2015.

[2] L. F. Yang, D. Q. Chu, L. M. Wang, H. L. Sun, and G. Ge, "Enhanced photocatalytic activity of porous cuprous oxide dodecahedron nanocrystals synthesized by solvothermal method," *Materials Letters*, vol. 159, pp. 172–176, 2015.

[3] X. H. Li, J. Q. Wang, Y. H. Zhang, and M. H. Cao, "Efficient visible-light photocatalytic performance of cuprous oxide porous nanosheet arrays," *Materials Research Bulletin*, vol. 70, no. 14, pp. 728–734, 2015.

[4] L. F. Li, W. X. Zhang, C. Feng, X. W. Luan, J. Jiang, and M. L. Zhang, "Preparation of nanocrystalline Cu_2O by a modified solid-state reaction method and its photocatalytic activity," *Materials Letters*, vol. 107, pp. 123–125, 2013.

[5] L. Xu, F. Y. Zhang, X. Y. Song, Z. L. Yin, and Y. X. Bu, "Construction of reduced graphene oxide-supported Ag-Cu_2O composites with hierarchical structures for enhanced photocatalytic activities and recyclability," *Journal of Materials Chemistry A*, vol. 3, no. 11, pp. 5923–5933, 2015.

[6] L. Xu, C. Srinivasakannan, J. H. Peng, M. Yan, D. Zhang, and L. B. Zhang, "Microfluidic reactor synthesis and photocatalytic behavior of Cu@Cu_2O nanocomposite," *Applied Surface Science*, vol. 331, pp. 449–454, 2015.

[7] L. Zhang, D. Jing, L. Guo, and X. Yao, "In situ photochemical synthesis of Zn-doped Cu_2O hollow microcubes for high efficient photocatalytic H_2 production," *ACS Sustainable Chemistry & Engineering*, vol. 2, no. 6, pp. 1446–1452, 2014.

[8] J. Zhang, W. X. Liu, X. W. Wang, X. Q. Wang, B. Hu, and H. Liu, "Enhanced decoloration activity by Cu_2O@TiO_2 nanobelts heterostructures via a strong adsorption-weak photodegradation process," *Applied Surface Science*, vol. 282, no. 2, pp. 84–91, 2013.

[9] J. Ma, K. Wang, L. Li, T. Zhang, Y. Kong, and S. Komarneni, "Visible light photocatalytic decolorization of Orange II on Cu_2O/ZnO nanocomposites," *Ceramics International*, vol. 41, no. 2, pp. 2050–2056, 2015.

[10] S. D. Sun, "Recent advances in hybrid Cu_2O-based heterogeneous nanostructures," *Nanoscale*, vol. 7, no. 25, pp. 10850–10882, 2015.

[11] P. Wang, B. B. Huang, X. Y. Qin et al., "Ag@AgCl: a highly efficient and stable photocatalyst active under visible light," *Angewandte Chemie, International Edition in English*, vol. 47, no. 41, pp. 7931–7933, 2008.

[12] F. P. Yan, Y. H. Wang, J. Y. Zhang, Z. Lin, J. S. Zheng, and F. Huang, "Schottky or ohmic metal–semiconductor contact: influence on photocatalytic efficiency of Ag/ZnO and Pt/ZnO model systems," *ChemSusChem*, vol. 7, no. 1, pp. 101–104, 2014.

[13] S. D. Sun, C. C. Kong, H. J. You, X. P. Song, B. J. Ding, and Z. M. Yang, "Facet-selective growth of Cu-Cu_2O heterogeneous architectures," *CrystEngComm*, vol. 14, no. 1, pp. 40–43, 2012.

[14] M. A. Mahmoud, W. Qian, and M. A. El-Sayed, "Following charge separation on the nanoscale in Cu_2O-Au nanoframe hollow nanoparticles," *Nano Letters*, vol. 11, no. 8, pp. 3285–3289, 2011.

[15] Z. H. Wang, S. P. Zhao, S. Y. Zhu, Y. L. Sun, and M. Fang, "Photocatalytic synthesis of M/Cu_2O (M = Ag, Au) heterogeneous nanocrystals and their photocatalytic properties," *CrystEngComm*, vol. 13, no. 7, pp. 2262–2267, 2011.

[16] X. L. Deng, C. G. Wang, E. Zhou et al., "One-step solvothermal method to prepare Ag/Cu_2O composite with enhanced photocatalytic properties," *Nanoscale Research Letters*, vol. 11, no. 1, p. 29, 2016.

[17] W. X. Zhang, X. N. Yang, Q. Zhu et al., "One-pot room temperature synthesis of Cu_2O/Ag composite nanospheres with enhanced visible-light-driven photocatalytic performance," *Industrial and Engineering Chemistry Research*, vol. 53, no. 42, pp. 16316–16323, 2014.

[18] N. Zhang, Y. H. Zhang, and Y. J. Xu, "Recent progress on graphene based photocatalysts: current status and future perspectives," *Nanoscale*, vol. 4, no. 19, pp. 5792–5813, 2012.

[19] M. Ahmad, E. Ahmed, W. Ahmed, A. Elhissi, Z. L. Hong, and N. R. Khalid, "Enhancing visible light responsive photocatalytic activity by decorating Mn-doped ZnO nanoparticles on graphene," *Ceramics International*, vol. 40, no. 7, pp. 10085–10097, 2014.

[20] Z. Jin, W. B. Duan, B. Liu, X. D. Chen, F. H. Yang, and J. P. Guo, "Fabrication of efficient visible light activated Cu–P25–graphene ternary composite for photocatalytic degradation of methyl blue," *Applied Surface Science*, vol. 356, pp. 707–718, 2015.

[21] S. H. Hsieh, W. J. Chen, and C. T. Wu, "Pt–TiO_2/graphene photocatalysts for degradation of AO7 dye under visible light," *Applied Surface Science*, vol. 340, pp. 9–17, 2015.

[22] M. M. Chen, Q. Y. Yang, L. F. Li, P. P. Xiao, M. Z. Liu, and M. L. Zhang, "Solid-state synthesis of $CuBi_2O_4$/MWCNT composites with enhanced photocatalytic activity under visible light irradiation," *Materials Letters*, vol. 171, pp. 255–258, 2016.

[23] W. W. Lu, S. Y. Gao, and J. J. Wang, "One-pot synthesis of Ag/ZnO self-assembled 3D hollow microspheres with enhanced photocatalytic performance," *Journal of Physical Chemistry C*, vol. 112, no. 43, pp. 16792–16800, 2008.

[24] C. Chen, W. M. Cai, M. C. Long et al., "Synthesis of visible-light responsive graphene oxide/TiO_2 composites with p/n heterojunction," *ACS Nano*, vol. 4, no. 11, pp. 6425–6432, 2010.

[25] X. Q. An, K. F. Li, and J. W. Tang, "Cu_2O/reduced graphene oxide composites for the photocatalytic conversion of CO_2," *ChemSusChem*, vol. 7, no. 4, pp. 1086–1093, 2014.